Supporting information for

Improve photocatalytic performance of metal–organic framework for CO_2 conversion by ligand modification

Xiuyan Cheng,[a, b] Jianling Zhang,*[a, b, c] Xiuniang Tan,[a, b] Lirong Zheng,[d] Dongxing Tan,[a, b] Lifei Liu,[a, b] Gang Chen,[a, b] Qiang Wan,[a, b] Bingxing Zhang,[a, b] Fanyu Zhang,[a, b] Zhuizhui Su,[a, b] Buxing Han[a, b, c] and Jing Zhang[d]

[a]Beijing National Laboratory for Molecular Sciences, CAS Key Laboratory of Colloid, Interface and Chemical Thermodynamics, CAS Research/Education Center for Excellence in Molecular Sciences, Institute of Chemistry, Chinese Academy of Sciences, Beijing 100190, P.R.China.

[b]School of Chemical Sciences, University of Chinese Academy of Sciences, Beijing 100049, P.R.China.

[c]Physical Science Laboratory, Huairou National Comprehensive Science Center, Beijing 101400, P.R.China.

[d]Beijing Synchrotron Radiation Facility (BSRF), Institute of High Energy Physics, Chinese Academy of Sciences, Beijing 100049, P.R.China.

*Corresponding author e-mail: zhangjl@iccas.ac.cn

Table of contents

Experimental

Materials.

Zirconium tetrachloride ($ZrCl_4$, > 99.95%) was obtained from Strem Chemicals, Inc. N,N-dimethylformamide (DMF, A.R. grade), ethanol (C_2H_5OH, A.R. grade), 2-aminoterephthalic acid (H_2ATA, 98%), triethanolamine (TEOA, > 99%), 1-(pyridin-4-yl)ethanone (> 98%) and isonicotinaldehyde (> 97%) were provided by Innochem Technology Co., Ltd. Acetic acid (A.R. Grade), acetonitrile (A.R. Grade), ammonium hydroxide (25%, A.R. Grade), anhydrous methyl alcohol (A.R. Grade) and ethanol (A.R. Grade) were purchased from Beijing Chemical Works. Deionized water was provided by Beijing Analysis Instrument Factory. Nafion D-521 dispersion (5% w/w in water and 1-propanol, ≥ 0.92 meq/g exchange capacity) was purchased from Alfa Aesar China Co., Ltd. Potassium hydroxide (KOH, > 85%) was provided by Alfa Aesar, a Johnson Matthery Company. N_2 (99.999%) and CO_2 (> 99.999%) were provided by Beijing Analysis Instrument Factory.

Synthesis of NH_2-UiO-66.

$ZrCl_4$ (0.15 g), acetic acid (5 mL) and H_2O (148 μL) were dissolved in 40 mL DMF under stirring at room temperature. After 2 h, H_2ATA (0.14 g) was added in the above solution with continuous stirring. Then the solution was transferred to a 50 mL Teflon-lined stainless steel autoclave, which was subsequently heated at 120 °C for 24 h. After cooling to ambient temperature, the product was collected by centrifugation and washed with DMF and methanol for three times. Finally, the product was dried in a vacuum oven at 80 °C for 12 h.

Synthesis of tpy.

Tpy was synthesized according to a previous report.[1] In brief, 1-(pyridin-4-yl)ethanone (50 mmol) was added to a solution of isonicotinaldehyde (25 mmol) in ethanol (200 mL). Potassium hydroxide (55 mmol) and ammonium hydroxide (25%, 144 mL) were added into the above solution in order. Subsequently, the red solution was stirred at room temperature for 24 h. The precipitate was collected by centrifugation, washed with water and ethanol for three times and dried in a vacuum oven at 80 °C for 12 h.

Synthesis of NH_2-UiO-66-tpy.

For the preparation of NH_2-UiO-66-tpy, a mixture of NH_2-UiO-66 (0.16 g) and tpy (0.10 g) were put into 8 mL DMF using a 15 mL Teflon-lined stainless steel autoclave, then sonicated for 20 min and vigorously stirred for 20 min to obtain a suspension. The mixture was heated at 190 °C for 14 h. After cooling to room temperature, the solid was collected by centrifugation, washed by DMF and methanol for three times and dried in a vacuum oven at 80 °C for 12 h.

Characterizations.

X-ray diffraction (XRD) was determined by a Rigaku D/max-2500 diffractometer equipped with Cu Kα radiation (λ = 1.5418 Å) at 40 kV and 200 mA. The morphologies of samples were observed on scanning electron microscope (SEM, HITACHI SU-8020), transmission electron microscope (TEM, JEOL JEM-1011) and high-resolution transmission electron microscope (HRTEM, JEOL-2100F) operated at 200 kV. The porosity properties were determined by an autosorb-iQ at 77 K using liquid nitrogen as coolant. The material was degassed at 120 °C for 6 h before the measurement. X-ray photoelectron spectroscopy (XPS) was carried out with a multipurpose X-ray photoemission spectroscope (Thermo Scientific ESCALAB 250Xi). Contact angle measurements were performed at 25 °C using a contact angle meter (HARKE-SPCAX1) by placing a water droplet on the surface of the sample film. The N content of each sample was measured twice on FLASH EA1112 elemental analysis instrument and the data error is 0.01 wt%. Fourier transform infrared (FT-IR) spectra were determined by a Bruker Tensor 27 spectrometer. The KBr pellet method was applied to prepare the solid sample. The optical absorption property was characterized by ultraviolet visible diffused reflectance spectrum (UV-Vis DRS, UV-2600, SHIMADZU) using $BaSO_4$ as a reference for diffuse experiments. Photoluminescence (PL) spectra were recorded at room temperature with a Hitachi F-4600 fluorescence spectrophotometer with the excitation wavelength of 320 nm. The time-resolved fluorescent decay spectroscopy (TRFDS) was performed on LifeSpec-II. X-ray absorption fine structure (XAFS) measurement for Zr K-edge was carried out at room temperature at the 1W1B beamline of the Beijing Synchrotron Radiation Facility (BSRF). For XAFS analysis, the extraction of the $\chi(k)$ function was performed using the Athena program. The averaged k^3-weight $\chi(k)$ function was Fourier transformed in the Δk = 2.589-12.300 $Å^{-1}$ interval with a Rbkg value of 1.0 and the uncorrected phase shift. The XANES spectrum was calibrated by setting the Zr K-edge energy to 17998 eV in the reference channel (Zr foil).

Electrochemical test.

The electrochemical measurement was implemented in a three-electrode system at electrochemical workstation (CHI660E, Chenhua Instrument, Shanghai, China) with the photocatalyst-coated indium-tin oxide (ITO) as the working electrode, an Ag/AgCl with 3.5 M KCl as a reference electrode and Pt net (1×1 cm) as the counter electrode. The illumination source adopted in photocurrent ON/OFF cycles was a 300 W Xe lamp with full spectrum. A 0.5 M Na_2SO_4 solution (pH = 6.8) was applied as electrolyte. To prepare the catalyst ink, 3 mg of the photocatalyst and 10 µL of 5 % Nafion 117 solution, as conducting binder, were introduced into 200 µL of ethanol and sonicated for 1 h. Then the catalyst ink was dropped on the surface of an ITO plate (1×1 cm^2) to prepare the working electrodes. Transient photocurrents, Mott-Schotty measurements and electrochemical impedance spectroscopy (EIS) Nyquist plots were performed in a 0.5 M Na_2SO_4 solution. All the potentials were recorded versus Ag/AgCl (*vs.* Ag/AgCl) electrode.

Photocatalytic CO_2 conversion.

In a typical experiment, 5 mg of NH_2-UiO-66-tpy and 100 µL of TEOA were dispersed in 5 mL of acetonitrile in a 100 mL round-bottom flask and vigorously stirred for 5 min to obtain a suspension. Then CO_2 (1 atm) was charged into the suspension for 30 min under stirring, which was placed in a water bath of 30 °C. The sample was irradiated by simulated solar irradiation with a 300 W Xe lamp (Aulight CEL-HX, Beijing) with a cut-off filter (*i.e.*, $350 < \lambda < 780$ nm). After the desired irradiation time, gas products were analyzed by gas chromatograph (GC, HP 4890D), which was equipped with thermal conductivity detector (TCD) and flame ionization detector (FID) using helium as internal standard.

The liquid products were analyzed by ^{1}H nuclear magnetic resonance (^{1}H NMR) spectroscopy (Bruker Avance Ⅲ 400 HD).

Computational method.

Density functional theory (DFT) calculations were performed using Vienna Ab-initio Simulation Package (VASP).[2,3] The projector augmented plane wave (PAW) method was used to describe the interactions between ion cores and valence electrons.[4,5] The electron exchange-correlation interaction was treated using the generalized gradient approximation (GGA) with the Perdew-Burke-Ernzerhof (PBE) functional. The plane waves with a cutoff energy of 400 eV were used and the 3×3×1 Monkhorst-Pack grid k-points were employed to sample the Brillouin zone integration. The structures were optimized until the energy and the force were converged to 1.0×10^{-5} eV/atom and 0.02 eV/Å, respectively. Over these optimized structures, vibrational frequencies were calculated in order to obtain zero-point energies (ZPE), thermal corrections and entropy contributions. All Gibbs free energy values for the CO_2 reduction mechanism were referenced to the Computational Hydrogen Electrode (CHE) model using the Proton-Coupled Electron Transfer (PCET) approach.

Results and Discussion

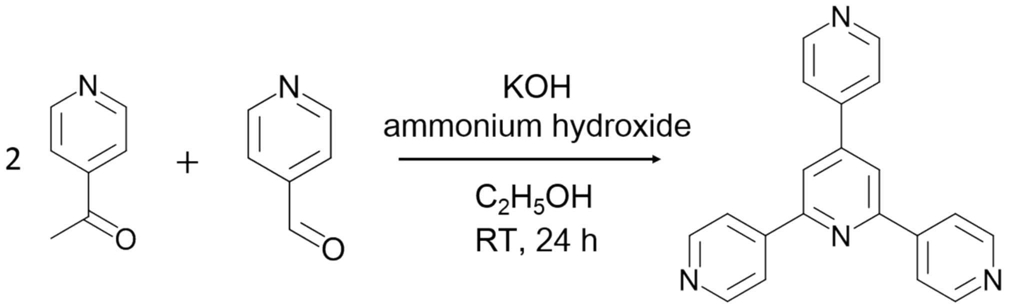

Fig. S1 Preparation of tpy. It can be easily synthesized at gram level in one batch at room temperature.[1] The average distance between terminal N atoms of tpy ligand is 9.78 Å (without considering Van der Waals radii).[6]

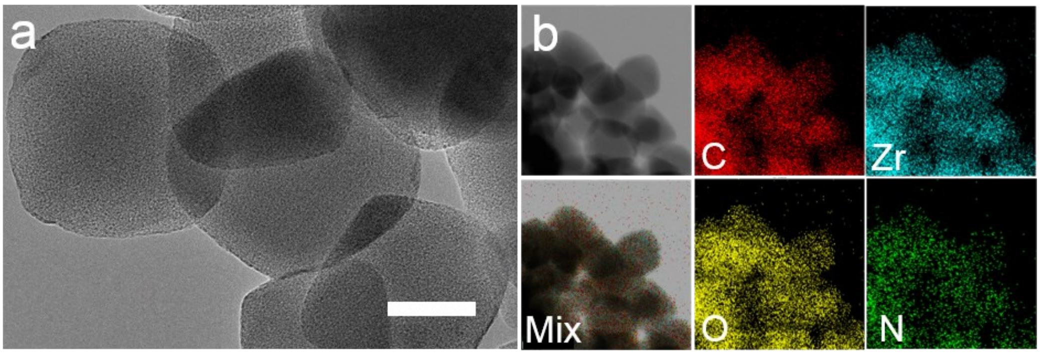

Fig. S2 TEM image (a) and EDS elemental mapping (b) of NH_2-UiO-66-tpy with tpy content of 6.2 wt%. Scale bar: 50 nm in (a).

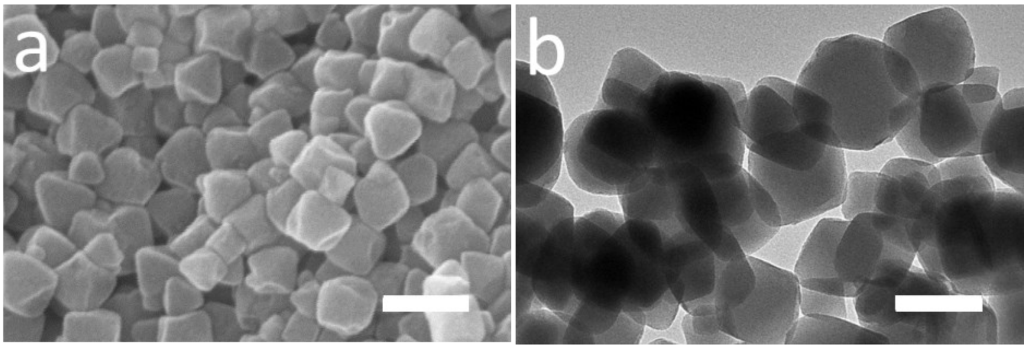

Fig. S3 SEM (a) and TEM (b) images of NH_2-UiO-66. Scale bars: 200 nm in (a), 100 nm in (b).

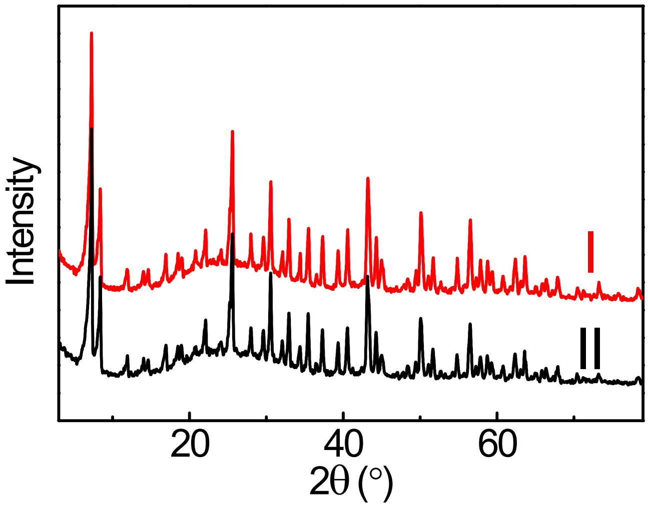

Fig. S4 XRD patterns of NH_2-UiO-66-tpy with tpy content of 6.2 wt% (I) and NH_2-UiO-66 (II).

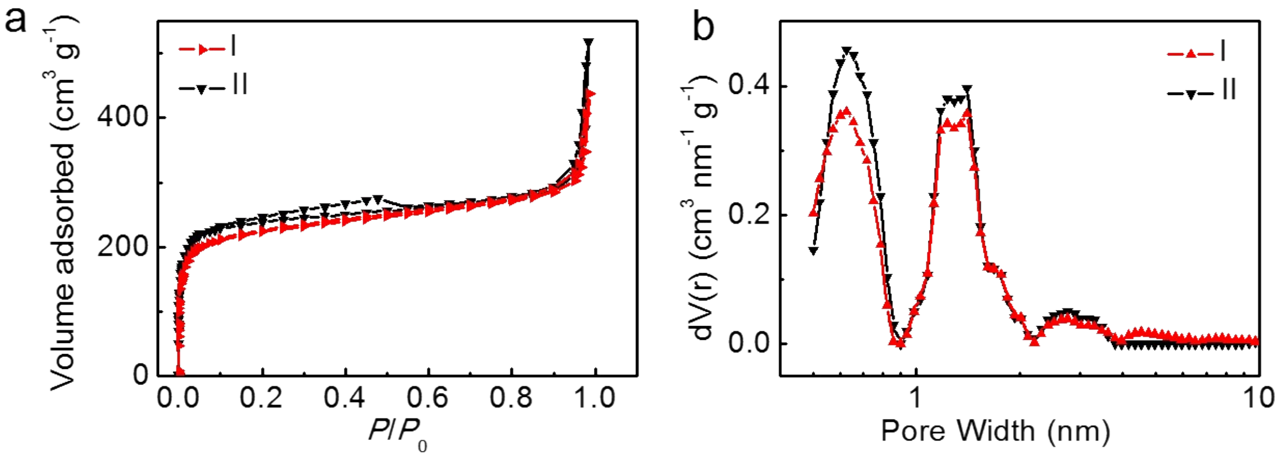

Fig. S5 N_2 adsorption-desorption isotherms (a) and pore size distribution curve (b) of NH_2-UiO-66-tpy with tpy content of 6.2 wt% (I) and NH_2-UiO-66 (II). The BET surface areas of NH_2-UiO-66-tpy and NH_2-UiO-66 are 857.2 and 941.9 m^2 g^{-1}, respectively. The pore size distribution curve of NH_2-UiO-66 was calculated from DFT analysis. It shows two major pore size distribution centered at about 0.6 and 1.3 nm.

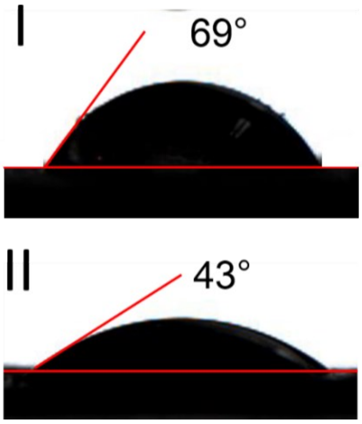

Fig. S6 Contact angles of NH_2-UiO-66-tpy with tpy content of 6.2 wt% (I) and NH_2-UiO-66 (II).

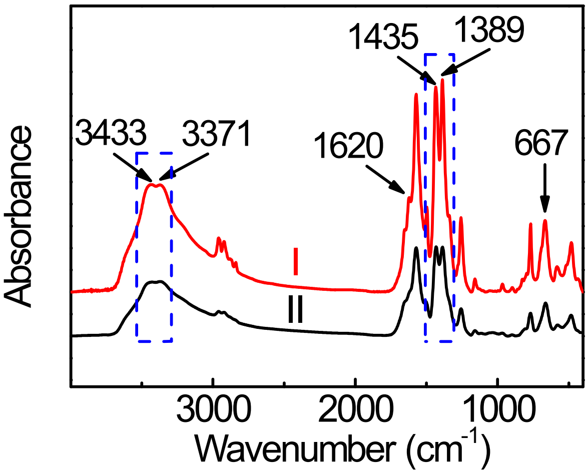

Fig. S7 FT-IR spectra of NH_2-UiO-66-tpy with tpy content of 6.2 wt% (I) and NH_2-UiO-66 (II). The absorption at 1572 cm^{-1} is assigned to the interaction of COO^- with Zr^{4+}.[7] The absorptions at 1258 and 1505 cm^{-1} are related to C-N stretching band and C=C vibration of benzene ring, respectively.[8] The absorptions between 600 and 800 cm^{-1} are referred to the Zr-O_2 longitudinal and transverse mode.[9] Compared with NH_2-UiO-66, a new absorption appears at 1620 cm^{-1} for NH_2-UiO-66-tpy, which can be assigned to the C=N stretch mode in tpy, confirming the successful doping of tpy in NH_2-UiO-66-tpy. Moreover, the absorption at 663 cm^{-1} of Zr-O_2 shifts to 667 cm^{-1}. It can be explained by the introduction of tpy, which changes the coordination environment of Zr and O. The absorptions at 3427 and 3367 cm^{-1} of the pristine NH_2-UiO-66 correspond to the asymmetric and symmetric vibrations of -NH_2 groups on the organic linker, respectively.[10] For NH_2-UiO-66-tpy, these two bands shift to higher wavenumbers (3433 and 3371 cm^{-1}, respectively). It implies that some bondings between the amino groups in the coordinated acid and the C=O groups of free organic ligand are broken.[11] Obviously, the symmetric stretching vibrations of the carboxylic groups show a blue shift from 1431 and 1387 cm^{-1} in NH_2-UiO-66 to 1435 and 1389 cm^{-1} in NH_2-UiO-66-tpy,[12] suggesting that nitrogen on tpy has a coordination effect with Zr-O clusters to form N-Zr-O bond.

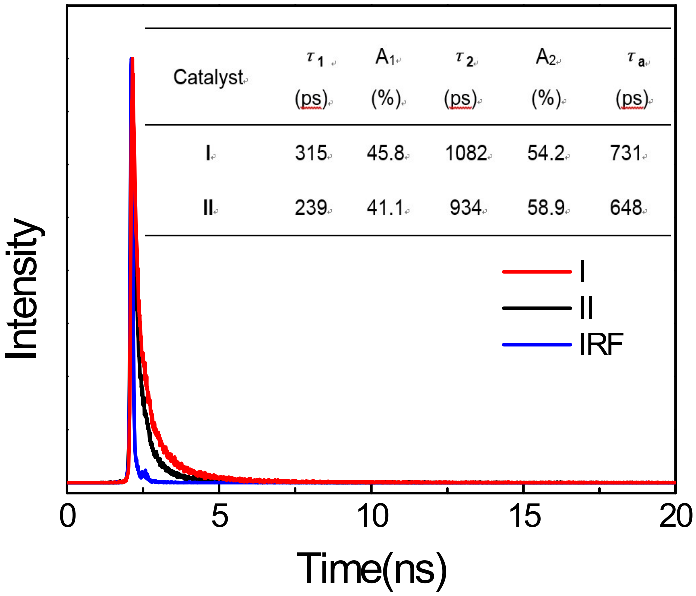

Catalyst	τ_1 (ps)	A_1 (%)	τ_2 (ps)	A_2 (%)	τ_a (ps)
I	315	45.8	1082	54.2	731
II	239	41.1	934	58.9	648

Fig. S8 TRFDS spectra of NH_2-UiO-66-tpy with tpy content of 6.2 wt% (I) and NH_2-UiO-66 (II).

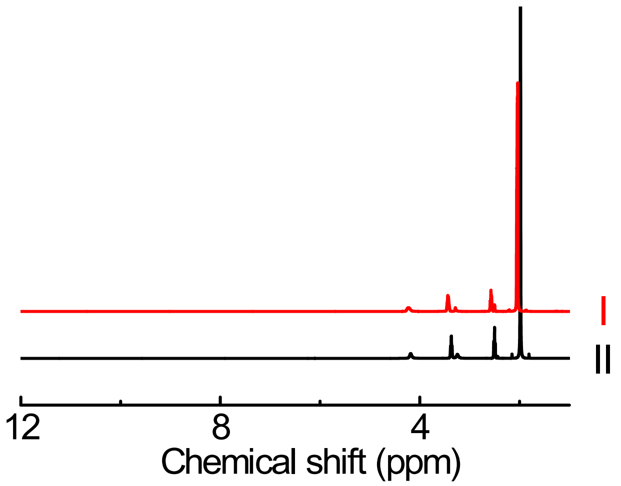

Fig. S9 ^{1}H NMR spectra of the liquid product after photocatalytic CO_2 reduction by NH_2-UiO-66-tpy with tpy content of 6.2 wt% (I) and NH_2-UiO-66 (II).

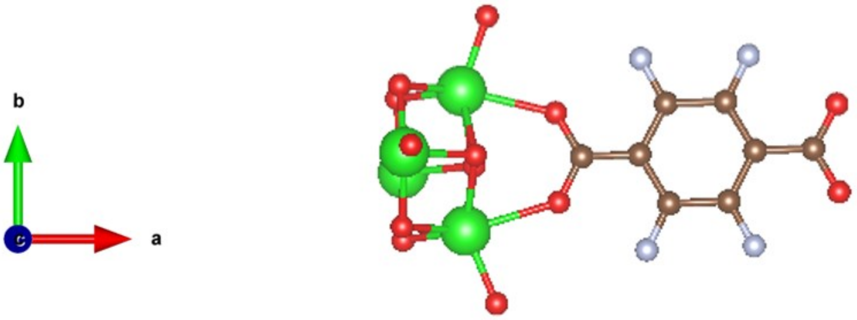

Fig. S10 Theoretical models of NH_2-UiO-66 used in DFT calculations.

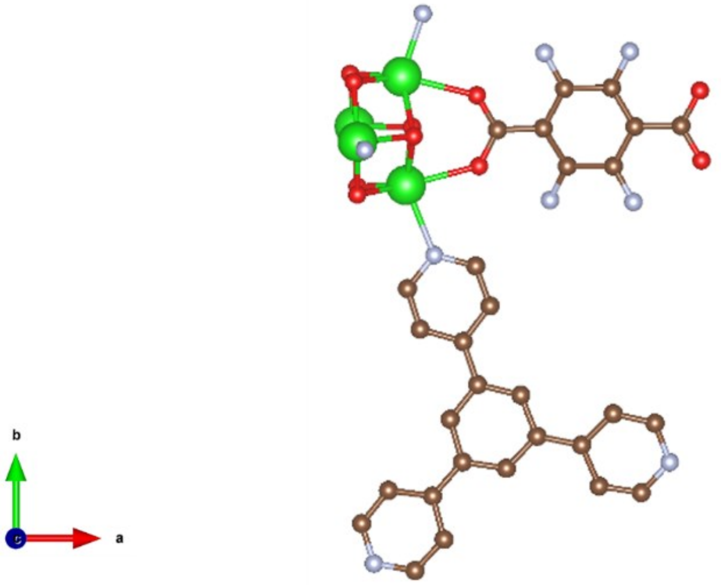

Fig. S11 Theoretical models of top view of NH_2-UiO-66-tpy used in DFT calculations.

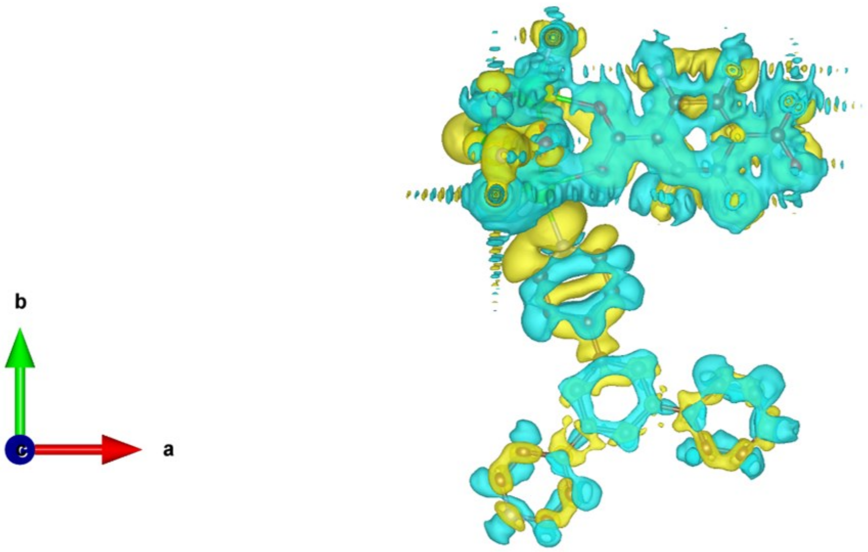

Fig. S12 Differential charge density of NH_2-UiO-66-tpy. The blue and yellow colours represent charge depletion and accumulation, respectively.

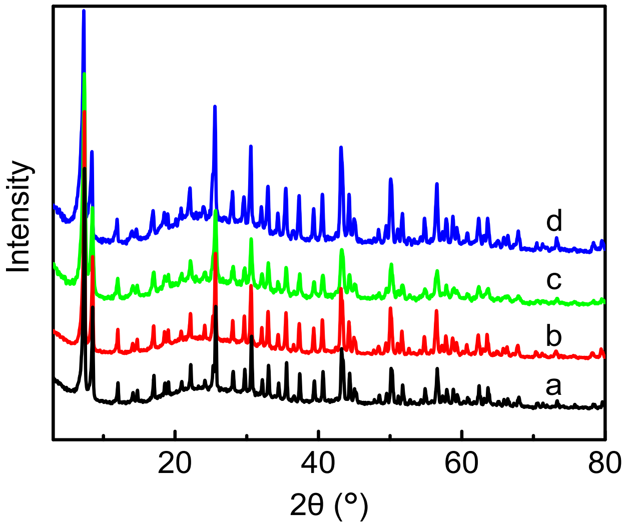

Fig. S13 XRD patterns of NH_2-UiO-66-tpy with different tpy contents of 0.6 wt% (a), 2.1 wt% (b), 3.9 wt% (c) and 7.1 wt% (d). By changing the tpy content from 0.6 wt% to 7.1 wt%, all the NH_2-UiO-66-tpy samples well retain the structure of NH_2-UiO-66.

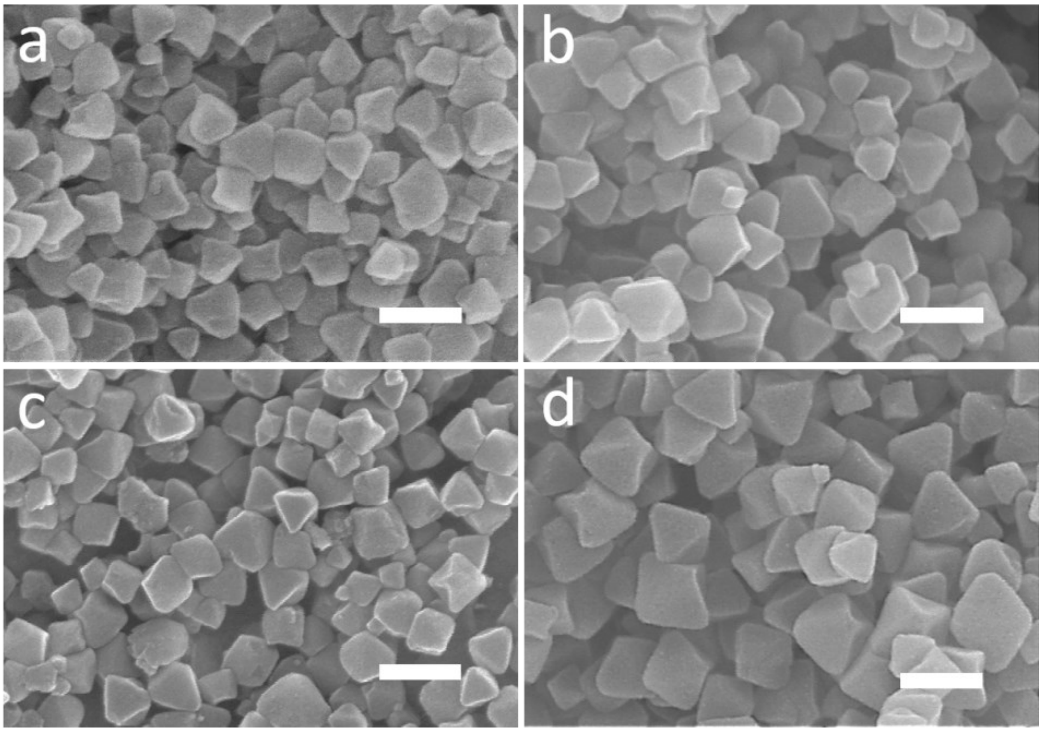

Fig. S14 SEM images of NH_2-UiO-66-tpy with different tpy contents of 0.6 wt% (a), 2.1 wt% (b), 3.9 wt% (c) and 7.1 wt% (d). Scale bar: 200 nm. By changing the tpy content from 0.6 wt% to 7.1 wt%, all the NH_2-UiO-66-tpy samples well retain the morphology of NH_2-UiO-66.

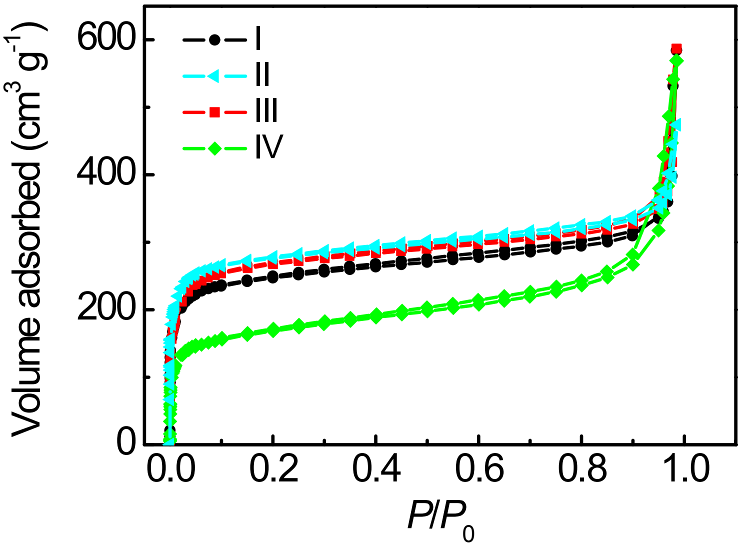

Fig. S15 N_2 adsorption-desorption isotherms NH_2-UiO-66-tpy with different tpy contents of 0.6 wt% (I), 2.1 wt% (II), 3.9 wt% (III) and 7.1 wt% (IV). By changing the tpy content from 0.6 wt% to 7.1 wt%, there is a large decrease in porosity for the NH_2-UiO-66-tpy sample with a tpy content of 7.1 wt%. It means that the excessive tpy would block up the micropores of NH_2-UiO-66.

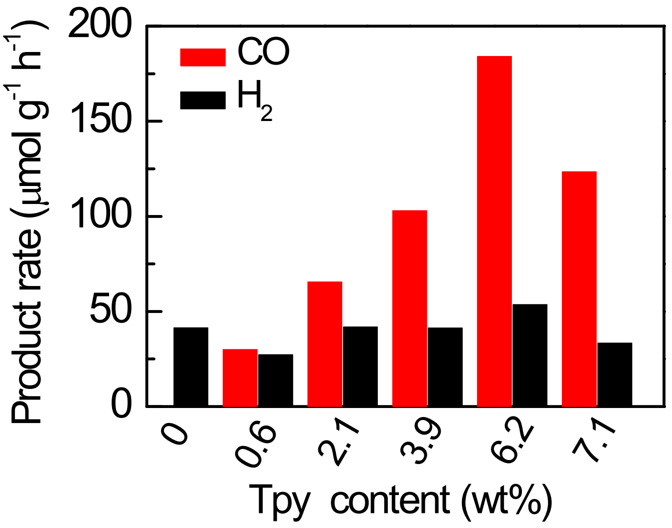

Fig. S16 Product rate catalyzed by NH_2-UiO-66 and NH_2-UiO-66-tpy with different tpy contents of 0.6 wt%, 2.1 wt%, 3.9 wt%, 6.2 wt% and 7.1 wt%. Reaction conditions: 5 mg catalyst, 5 mL acetonitrile, 0.5 g triethanolamine, simulated solar irradiation with a 300 W Xe lamp with a cut-off filter (*i.e.*, 350 < λ < 780 nm). The CO production rates catalyzed by the different samples increase first and then decrease with increasing tpy amount in the NH_2-UiO-66-tpy catalysts. When the tpy content is 6.2 wt%, the CO evolution rate reaches the maximum. This indicates that a sufficient amount of tpy in NH_2-UiO-66-tpy is needed for the optimum photocatalytic CO_2RR, while an excess amount of tpy impedes the CO_2RR by blocking the effect of tpy on NH_2-UiO-66.

Table S1 Comparison of the reaction conditions and performances of different catalysts for photocatalytic CO_2 reaction to CO.

Catalysts	Co-catalysts	Conditions [a]	Light source	Time (h)	Carbon products rate ($\mu mol\ g^{-1}\ h^{-1}$)	Ref.
UiO-66/CNNS	-	MeCN/TEOA solution (5 mL, v/v: 4:1), CO_2: 0.80 atm	Visible light: 300 W Xe lamp with a cut-off filter ($400 < \lambda < 800$ nm)	6	CO: 9.8	13
CdS/NH_2-UiO-66 membrane (16.5 mg)	bipyridine (10 mg)	MeCN/H_2O/TEOA solution (18 mL, v/v/v: 3:2:1)	Visible light: 300 W Xe lamp with a cut-off filter ($400 < \lambda < 760$ nm)	6	CO: 87.0	14
holey g-C_3N_4 (HGN)/NH_2-UiO-66 (NUZ) (10 mg)	-	H_2O/TEOA solution (30 mL, v/v: 20/1), CO_2: 0.80 atm	Visible light: 300 W Xe lamp with a cut-off filter ($400 < \lambda < 800$ nm)	12	CO: 31.6	15
TiO_2/NH_2-UiO-66 [b] (3 mg)	-	CO_2/H_2 (v/v: 3/2), CO_2: 1.15 atm	UV-Vis light: 150 W Xe lamp with a cut-off filter ($\lambda > 325$ nm)	6	CO: 5.3	16
$CsPbBr_3$ QDs/UiO-66-NH_2 (10 mg)	-	H_2O/ethylacetate solution (30 mL, v/v: 1/300), CO_2: 0.80 atm	Visible light: 300 W Xe lamp with a cut-off filter ($420 < \lambda < 800$ nm)	12	CH_4: 0.3 CO: 8.2	17
CdS/UiO-bpy/Co (10 mg)	-	MeCN/TEOA solution (3 mL, v/v: 6/1)	Visible light: 300 W Xe lamp with a cut-off filter ($420 < \lambda < 800$ nm).	10	CO: 195	18

Co-ZIF-9 (0.8 μmol)	$[Ru(bpy)_3]Cl_2$ (10.0 μmol)	MeCN/H_2O solution (5 mL, v/v: 4/1), TEOA (1 mL)	Visible light: 300 W Xe lamp with a cut-off filter ($\lambda \geq 420$ nm)	0.5	CO: 41.8	19
MOF-525-Co [c] (2 mg)	-	MeCN/TEOA solution (2 mL, v/v: 4/1)	Visible light: 300 W Xe lamp with a cut-off filter ($400 < \lambda < 800$ nm)	6	CO: 201.6 CH_4: 36.7	20
MOF 4 (UiO-67 doped with $Re(bpy)(CO)_3Cl$ complexes)	-	MeCN/TEA solution (2.1 mL, v/v: 20/1)	UV light: 450 W Xe lamp with a cut-off filter ($\lambda > 300$ nm)	6	CO: TON = 5.0 [d]	21
Re-MOF-NH_2 (5 mg)	-	0.1 mL TEA	Visible light: 300 W Xe lamp with a cut-off filter ($400 < \lambda < 700$ nm)	6	CO: 1.1	22
NH_2-MIL-101 (Fe) NH_2-MIL-53 (Fe) NH_2-MIL-88B (Fe) (2 mg)	-	2 mL TEOA, solvent-free reaction system	Visible light: 300 W Xe lamp with a cut-off filter ($400 < \lambda < 780$ nm)	5	CO: 17.5 CO: 3.1 CO: 10.8	23
NH_2-UiO-66 (5 mg)	-	MeCN/TEOA solution (5 mL, v/v: 11/1)	Simulate sunlight: 300 W Xe lamp with a cut-off filter ($350 < \lambda < 780$ nm)	8	CO: 34.0	This work
NH_2-UiO-66-tpy (5 mg)	-	MeCN/TEOA solution (5 mL, v/v: 11/1)	Simulate sunlight: 300 W Xe lamp with a cut-off filter ($350 < \lambda < 780$ nm)	8	CO: 209.2	This work

[a] The pressure of CO_2 is 1 atm in the photocatalytic CO_2 reduction reaction. [b] It was performed in a gas/solid reactor setup and photocatalyst illumination area was 4.5 cm^2. [c] Porphyrin based MOF. [d] TON of CO is defined as the number of evolved CO molecules per catalytic site.

References

1. Y.-S. Wei, M. Zhang, M. Kitta, Z. Liu, S. Horike and Q. Xu, *J. Am. Chem. Soc.*, 2019, **141**, 7906–7916.
2. G. Kresse and J. Hafner, *Phys. Rev. B*, 1993, **47**, 558–561.
3. G. Kresse, and J. Hafner, *Phys. Rev. B*, 1994, **49**, 14251–14269.
4. P. E. Blochl, *Phys. Rev. B*, 1994, **50**, 17953–17979.
5. G. Kresse, and D. Joubert, *Phys. Rev. B*, 1999, **59**, 1758–1775.
6. H. Wang, J. Xu, D.-S. Zhang, Q. Chen, R.-M. Wen, Z. Chang and X.-H. Bu, *Angew. Chem., Int. Ed.*, 2015, **54**, 5966–5970.
7. R. Bibi, Q. H. Shen, L. F. Wei, D. D. Hao, N. X. Li and J. C. Zhou, *RSC Adv.*, 2018, **8**, 2048–2058.
8. C. S. Hinde, W. R. Webb, B. K. J. Chew, H. R. Tan, W.-H. Zhang, T. S. A. Hor and R. Raja, *Chem. Commun.*, 2016, **52**, 6557–6560.
9. E. F. López, V. S. Escribano, M. Panizza, M. M. Carnasciali and G. Busca, *J. Mater. Chem.*, 2001, **11**, 1891–1897.
10. F. Vermoortele, R. Ameloot, A. Vimont, C. Serre and D. D. Vos, *Chem. Commun.*, 2011, **47**, 1521–1523.
11. F. Y. Zhang, X. X. Sang, X. N. Tan, C. C. Liu, J. L. Zhang, T. Luo, L. F. Liu, B. X. Han, G. Y. Yang and B. P. Binks, *Langmuir*, 2017, **33**, 12427–12433.
12. J. H. Cavka, S. Jakobsen, U. Olsbye, N. Guillou, C. Lamberti, S. Bordiga and K. P. Lillerud, *J. Am. Chem. Soc.*, 2008, **130**, 13850–13851.
13. L. Shi, T. Wang, H. B. Zhang, K. Chang and J. H. Ye, *Adv. Funct. Mater.*, 2015, **25**, 5360–5367.
14. H. Zhao, X. Yang, R. Xu, J. J. Li, S. Y. Gao and R. Cao, *J. Mater. Chem. A*, 2018, **6**, 20152–20160.
15. Y. N. Wang, L. N. Guo, Y. Q. Zeng, H. W. Guo, S. P. Wan, M. Ou, S. L. Zhang and Q. Zhong, *ACS Appl. Mater. Interfaces*, 2019, **11**, 30673–30681.
16. A. Crake, K. C. Christoforidis, A. Kafizas, S. Zafeiratos and C. Petit, *Appl. Catal., B*, 2017, **210**, 131–140.
17. S. P. Wan, M. Ou, Q. Zhong and X. M. Wang, *Chem. Eng. J.*, 2019, **358**, 1287–1295.
18. C. J. Chen, T. B. Wu, H. H. Wu, H. Z. Liu, Q. L. Qian, Z. M. Liu, G. Y. Yang and B. X. Han, *Chem. Sci.*, 2018, **9**, 8890–8894.
19. S. B. Wang, W. S. Yao, J. L. Lin, Z. X. Ding and X. C. Wang, *Angew. Chem., Int. Ed.*, 2014, **53**, 1034–1038.
20. H. B. Zhang, J. Wei, J. C. Dong, G. G. Liu, L. Shi, P. F. An, G. X. Zhao, J. T. Kong, X. J. Wang, X. G. Meng, J. Zhang and J. H. Ye, *Angew. Chem., Int. Ed.*, 2016, **55**, 14310–14314.
21. C. Wang, Z. G. Xie, K. E. DeKrafft and W. B. Lin, *J. Am. Chem. Soc.*, 2011, **133**, 13445–13454.
22. U. J. Ryu, S. J. Kim, H.-K. Lim, H. Kim, K. M. Choi and J. K. Kang, *Sci. Rep.*, 2017, **7**, 612.
23. X.-Y. Dao, J.-H. Guo, Y.-P. Wei, F. Guo, Y. Liu and W.-Y. Sun, *Inorg. Chem.*, 2019, **58**, 8517–8524.